# Selenium Compounds Affect Differently the Cytoplasmic Thiol/Disulfide State in Dermic Fibroblasts and Improve Cell Migration by Interacting With the Extracellular Matrix

Christine Kreindl , Sandra Soto-Alarcón , Miltha Hidalgo , Ana Riveros , Carolina Añazco , Rodrigo Pulgar , Omar Porras *

Posted Date: 15 December 2023

doi: 10.20944/preprints202312.1141.v1

Keywords: hyper biosensor; sodium selenite, selenium cysteine; selenium methionine; extracellular matrix; human dermic fibroblast; cellular migration

*Article*

# Selenium Compounds Affect Differently the Cytoplasmic Thiol/Disulfide State in Dermic Fibroblasts and improve Cell Migration by Interacting with the Extracellular Matrix

**Christine Kreindl [1], Sandra A. Soto-Alarcón [2], Miltha Hidalgo [1], Ana L. Riveros [3], Carolina Añazco [4], Rodrigo Pulgar [5] and Omar Porras [1,*]**

[1] Laboratory for Research in Functional Nutrition, Instituto de Nutrición y Tecnología de los Alimentos, Universidad de Chile, Chile; ntakreindl@gmail.com (C.K.); miltha.hidalgo@inta.uchile.cl (M.H.); omar.porras@inta.uchile.cl (O.P.)

[2] Nutrition and Dietetics, Faculty of Health Sciences, Universidad Autónoma de Chile, Chile; sandra.soto.alarcon@gmail.com (S.S.)

[3] Laboratorio de Nanobiotecnología y Nanotoxicología, Departamento de Química Farmacológica y Toxicológica, Facultad de Ciencias Químicas y Farmacéuticas, Universidad de Chile. Sergio Livingston 1007, Santiago 8380492, Chile; riveros.ana@gmail.com (A.R.)

[4] Laboratorio de Bioquímica Nutricional, Escuela de Nutrición y Dietética, Carrera de Nutrición y Dietética, Facultad de Ciencias para el Cuidado de la Salud, Universidad San Sebastián, General Lagos #1190, Valdivia 5110773, Chile; carolina.anazco@uss.cl (C.A.)

[5] Laboratory of Genomics and Genetics of Biological Interactions, Instituto de Nutrición y Tecnología de los Alimentos (INTA), Universidad de Chile, Santiago 7830490, Chile; rpulgar@inta.uchile.cl (R.P.)

* Correspondence: omar.porras@inta.uchile.cl ; Tel.: +56-2-9678-1583

**Abstract:** Deficient wound healing is frequently observed in patients diagnosed with diabetes, a clinical complication that compromises mobility and leads to limb amputation, decreasing patient autonomy and family lifestyle. Fibroblasts are crucial for secreting the extracellular matrix to pave the wound site for endothelial and keratinocyte regeneration. The biosynthetic pathways for collagen production are one of the main components of the extracellular matrix, as the crosslinking of extracellular collagen fibers is intimately related to fibroblast redox homeostasis. In this study, human dermic fibroblasts were cultured with 1 mM sodium selenite (inorganic) and 1 mM of two selenium amino acids (organic), Se-cysteine and Se-methionine. This concentration was compatible with long-term exposure necessary for extracellular matrix production and allowed us to examine the impact of these three compounds on the state and response of the thiol-based HyPer biosensor expressed in the cytoplasm. In addition, the abundance of extracellular matrix and ultrastructural properties were evaluated by Picrus Sirius red staining and scanning electronic microscopy, respectively. We also evaluated whether these selenium compounds effectively ameliorated the perturbations induced by culturing fibroblasts at high glucose levels (25 mM) regarding cytoplasmic redox, extracellular matrix and glycation on collagen fibers. Our results indicate that cytoplasm protein oxidation was sensitive to selenium compound supplementation. Selenium amino acids increased the sensitivity to protein oxidation, and only Se-cysteine increased the disulfide bond reduction in fibroblasts maintained in high glucose. Despite the lack of effect of selenium compounds on the glucose-induced increase in matrix fiber thickness, we found that endothelial migration improved in the matrix generated by high glucose-cultured fibroblasts.

**Keywords:** HyPer biosensor; sodium selenite; selenium cysteine; selenium methionine; extracellular matrix; human dermic fibroblast; cellular migration

## 1. Introduction

 doi:10.20944/preprints202312.1141.v1



The prevalence of type II diabetes has increased by 50% in the last ten years [1]. One of the hallmarks of this disease is sustained hyperglycemia that leads to unspecific and extensive modification of lysine residues on proteins by Schiff base reaction known as glycation [2]. Clinical complications, such as neuropathies, retinopathies, nephropathies, or diabetic foot ulcers, are related to the glycation degree observed in circulating haemoglobin [3]. Accumulative glycation on Extracellular Matrix (ECM) proteins [4,5] exerts a negative influence on the endothelial function at the microvascular level [6] as one of the pathogenic mechanisms for peripheral organ failure observed in diabetes.

The biosynthesis of collagen, one of the most abundant proteins in the ECM [7], enzymatic hydroxylation on immature collagen requires ascorbic acid at the endoplasmic reticulum of fibroblasts [8]. The extracellular maturation of collagen fibers requires enzymatic crosslinking by lysyl oxidase (LOX) to generate fibrils. Sustained circulating high glucose levels increases intracellular ROS production, likely by activating NADP(H) oxidase [9,10] and upregulating LOX [11,12], which together modify the mechanical properties of fibers [13,14]. Increased ECM stiffness, due to excessive crosslinking of fibers, decreases endothelial cell adhesion due to deficient anchoring of integrins with glycated proteins [15].

The antioxidant function of selenoproteins is well-supported by enzymes that regulate intra- and extracellular redox [16]. One of these selenoenzymes is the glutathione peroxidase (GPx), whose primary function is to convert hydrogen peroxide into water by oxidizing the selenol (-SeH) group to selenic acid (-SeOH), which is reduced back by glutathione [17]. In subjects with early arterial thrombosis, a 50% decrease in the activity of GPx3 has been associated with lower levels of ON [18], frequently present in subjects with diabetes type 2 [19]. On the other hand, thioredoxin reductase (TrxR) reduces disulfide bonds on thioredoxin proteins, thereby maintaining the homeostasis of -SH groups [20]. The TrxR system is relevant for counteracting the oxidative stress generated by high glucose. For instance, fibroblasts from Txnrd1 $^{-/-}$ mice were more sensitive to pharmacological GSH depletion than wild-type fibroblasts at 25 mM glucose, indicating that TrxR1 is indispensable for cell survival and the elimination of $H_2O_2$ under high-glucose conditions [20]. Selenium can be incorporated into proteins such as selenocysteine (SeCys) or selenomethionine (SeMet). For SeCys, which participates in the active site of GPx1, its incorporation is determined by the location of the UGA codon in the transcript [21] and several modifications on the anticodon loop in the transfer RNA [22]. The silencing of the tRNA gene encoding selenocysteine in mice provokes general skin disorders, including aberrant hair follicle morphogenesis, hyperplastic epidermis, and progressive alopecia [23]. By adding ~30 nM to the mesenchymal stem cells, Heo demonstrated increased proliferation of these cells and enhanced anti-inflammatory and angiogenic properties of the secreted exosomes *in vitro* and *in vivo* [24]. Recently, other groups have demonstrated that topical application with inorganic selenium improved wound healing and collagen deposition in animal models [25–30]. However, it is still unclear if the selenium carrier, inorganic versus organic, is relevant for ECM production and its redox impact on living human fibroblasts. Selenium compounds, such as $Na_2SeO_3$, SeCys, and SeMet, have not been employed in cell culture for durations exceeding 72 hours [31–33].

In this study, we evaluated if the supplementation with selenium amino acids (organic) and sodium selenite (inorganic) had an impact on the cytoplasmic oxidation/reduction balance of human dermic fibroblasts maintained at two glucose levels, 5 and 25 mM. By monitoring the HyPer signal, a fluorescent redox biosensor whose emission spectra change according to the disulfide/thiol state of a pair of cysteine residues, we corroborated that 25 mM glucose promoted a more oxidative cytoplasmic environment and that these fibroblasts produce a morphologically different ECM that offers reduced migration to endothelial cells to close a gap *in vitro*. Further experiments were done on purified collagen fibers to determine that SeCys and sodium selenite were effective in counteracting the effect of methylglyoxal-induced glycation.

## 2. Materials and Methods

Cell culture: The CCD-1068Sk fibroblast line (ATCC® CRL-2086™, USA) corresponds to normal mammary dermal tissue collected from a mastectomy procedure for mammary carcinoma. Cultures

 doi:10.20944/preprints202312.1141.v1



were maintained in Minimum Essential Media (MEM) (Life Technologies, Carlsbad, NY, USA) supplemented with a 10% fetal bovine serum (Corning Inc, New York, USA) and a 1% pen-strep solution (penicillin 10 000 U/mL-streptomycin 10 mg/mL, (Biological Industries, USA) under a humidified atmosphere at 37ºC and 5% $CO_2$. The cultures used were between passages 10 and 25. Cells were maintained in normal (5 mM) (NG) or high (25 mM) (HG) glucose concentrations for at least three passages. Ascorbic acid (155 µM) (Sigma-Aldrich, St. Louis, MO, USA) was added to the medium for ten days to promote collagen synthesis [34]. The human dermal microvasculature cell line, TIME (CRL-4025TM, ATCC, USA) was maintained at 37°C in M131 medium, enriched with Microvascular Endothelial Cell Growth Kit-VEGF, penicillin-streptomycin, and amphotericin under a humidified atmosphere with 5% $CO_2$. Culture media was renewed every 2 to 3 days, and cells were used between passages 3 and 10. Viability assays were performed on 12-well plates at cell confluence to choose the non-lethal concentration of selenium compounds. A range of concentrations (0.25-50 µM) of inorganic selenium (sodium selenite, SS) (Sigma-Aldrich, St. Louis, MO, USA), as well as organic selenium (selenomethionine, SeMet) Cayman Chemicals Company (Ann Harbor, MI, USA) and selenocysteine, (SeCys) (Sigma-Aldrich, St. Louis, MO, USA) was applied for ten days. Viable cells were identified by observation with the Neubauer chamber using trypan blue (Sigma-Aldrich, St. Louis, MO, USA) [35].

### *2.1. HyPer biosensor imaging*

HyPer is a fluorescent biosensor oxidized only by $H_2O_2$, which contains a pair of cysteines that, upon oxidation, induces a conformational change in its structure, resulting in altered spectral properties of the fluorescent domains [36]. This phenomenon is reversible and can be reduced by thioredoxin and glutathione reductase [37–39]. CCD1068Sk cells were seeded on glass coverslips for these experiments and subsequently infected with Adeno-HyPer (at a 1:50 dilution). After 48 hours, biosensor recordings were carried out using a Nikon TI Eclipse inverted epifluorescence microscope with a 40X objective [NA 1.3]. This microscope was connected to a xenon lamp and a monochromator (Cairn Research Ltd, Faversham, UK), allowing dual excitation at 420 and 490 nm. Emitted fluorescence was collected over 520 nm using a LongPass filter. The biosensor signal was expressed as a 490/420 ratio. On the day of the experiment, the culture medium was replaced with KRH buffer (in mM: 140 NaCl, 4.7 KCl, 20 HEPES, 1.25 $MgSO_4$, 1.25 $CaCl_2$, pH 7.4), supplemented with 5 mM glucose, and the coverslip was mounted in an open recording chamber. The hyPer ratio signal was recorded for a minimum of 15 minutes until a stable baseline was observed. We provoked the maximal oxidation of HyPer by applying a 500 µM $H_2O_2$ pulse (5 minutes), which, after being washed out, allowed the kinetic evaluation of the biosensor signal recovery.

### *2.2. Analysis of gene expression*

The RNA from fibroblasts was isolated with RNA-Solv® Reagent (Omega Bio-Tek Inc, USA ). Complementary DNA was generated by M-MLV reverse transcriptase (Promega, Madison, WI, USA) using oligo (dT) (Promega) using 1 µg of total RNA. Semiquantitative PCR reactions were performed using the following primers:

GPX1, forward 5′-TATCGAGAATGTGGCGTCCC-3′ and reverse 5′-TCTTGGCGTTCTCCTGATGC-3′, PCR product size 143 bp; TXNRD1, forward 5′-ATCATCATTGGAGGTGGCTCAG -3′ and reverse 5′-ACACATGTTCCTCCGAGACC-3′, PCR product size 134 bp; AQP1, forward 5′- AGGCTACAAAGCAGAGATCGAC-3′and reverse 5′-CACCCTCTAAATGGCTTCATTC -3, PCR product size 197 bp, PRDX1, forward 5′-GGGAACCTGGTTGAACCCC -3′ and reverse 5′- TGGCATAACAGCTGTGGCTT -3′, PCR product size 99 bp, B-ACTIN, forward 5′-GGAGCGAGATCCCTCCAAAAT-3′and reverse 5′-GGCTGTTGTCATACTTCTCATGG-3, PCR product size 197 bp,

Messenger expression was determined by real-time qPCR using AriaMx Real-Time PCR System (Agilent Technologies), and the amplification was performed with 200 ng of cDNA and a DNA Master SYBR® Green I reaction mix in a final volume of 20 µL. All reactions carried out were duplicated, including a negative control. Data was relativized to the expression of the messenger of

 doi:10.20944/preprints202312.1141.v1



β-actin. The relative expression of each studied gene was determined by the equation described in [40].

*2.3. Picrus Sirius Red staining*

CCD1068Sk cells were seeded on culture plates and maintained under the above-described experimental conditions. Cultures were decellularized with lysis buffer (Triton 0.5% *v/v* is 20 mM $NH_4OH$ solution), and samples were then fixed with 4% formaldehyde in PBS for 20 minutes. A 1 mg/mL concentration solution of Picrus Sirius Red (PSR) (Sigma-Aldrich, St. Louis, MO, USA) was added. The samples were washed twice with 0.5% acetic acid solution (0.5%) Merck (Darmstadt, Germany)., and at least 18 images were taken from each condition under a brightfield microscope images were collected. The area covered with fibers was obtained on fixed and stained decellularized samples with Image J software (v. Fiji)[41].

*2.4. Determination of fiber thickness by scanning electron microscope (SEM)*

After running the protocol for collagen synthesis on 12 mm coverslips, the cultures were decellularized, and the cell-free surface was fixed. In brief, the matrices were fixed for 12 hours using a PBS solution composed of 2% glutaraldehyde (Sigma-Aldrich, St. Louis, MO, USA), 1 M sodium cacodylate (Sigma-Aldrich, St. Louis, MO, USA), 0.1 M sucrose (Sigma-Aldrich, St. Louis, MO, USA). Subsequently, the samples were washed with a 0.1 M sodium cacodylate solution, followed by immersion in a 1% osmium tetroxide (Sigma-Aldrich, St. Louis, MO, USA) in 0.1 M sodium cacodylate solution for 1 hour. After this period, the solution was replaced with 1% tannic acid in 0.1 M sodium cacodylate solution for one hour more. Finally, the samples were dehydrated with ethanol and immersed in hexamethyldisilazane (Sigma-Aldrich, St. Louis, MO, USA) for 3 minutes [42]. After coating the samples with gold (10 nM), they were observed in a LEO 1420VP SEM equipped with a dispositive for surface element microanalysis and a linear profile at 10 kV and in a Tesla 343 A SEM instrument. Fiber thickness, number of branches and crosslinking were analyzed using the open-access software Image J (v. Fiji)[41].

*2.5. Cellular migration assay*

A wound-type assay was performed with endothelial cells seeded on two types of surfaces: decellularized surfaces and purified collagen type I. An intra-chamber device (abcam, UK) prevented the extracellular matrix disruption. To generate a surface covered with the collagen, 0.5 mg/mL human collagen type I (Corning Inc, New York, USA) in Phosphate-Buffered Saline (PBS 137 mM NaCl, 2.7 mM KCl, 8 mM $Na_2HPO_4$, and 2 mM $KH_2PO_4$) was adjusted to pH of 7.0-7.2. Polymerization was carried out for 2 hours at 37°C on 24-well culture plates. Glycation was performed with 10 mM methylglyoxal (MGO) in the presence or absence of 1 μM of selenium compounds overnight at 37°C in a humidified environment.

The endothelial cells were seeded on decellularized matrices or purified collagen until cells reached 90% confluence. At this time, the intra-chamber device was carefully lifted, and cells were gently washed twice with warm PBS. Images were taken under brightfield microscopy at the beginning (zero time) and 8 hours later. Then, the area of the existent gap was measured by Image J software (v Fiji)[41].

*2.6. Statistical analysis*

All data presented correspond to average ± SE from at least three independent experiments. Comparison of more than two experimental groups was analyzed by ANOVA, with Bonferroni post-hoc test, for non-parametric Kruskal-Wallis with Dunn´s post-hoc and averages between two groups with t-student. Tests were performed with 3 independent samples and at least 3 technical replicates under the described experimental conditions. Data plotting and analysis were done with GraphPad Prism 8 software.

Preprints (www.preprints.org) | NOT PEER-REVIEWED | Posted: 15 December 2023 doi:10.20944/preprints202312.1141.v1



## 3. Results

### *3.1. HyPer responses in human dermal fibroblasts culturing in normal and high glucose.*

HyPer biosensor was expressed in two groups of CCD-1068Sk cells, one maintained at 5 mM glucose (normal, NG) and the other at 25 mM glucose (high glucose, HG). Figure 1A,B show the classic response of the biosensor when 500 μM $H_2O_2$ is added to the extracellular space; this stimulus provokes a rapid increase in the ratio signal until a plateau is reached. Then, after removing the oxidant agent from the extracellular space, a recovery phase is followed, driving the signal back to basal values. Basal values of HyPer were compared between fibroblasts maintained at 5 and 25 mM glucose; cells maintained at normal glucose elicited values significantly lower than those cultured at 25 mM glucose (Figure 1C). Despite this difference, the oxidation rate of HyPer was similar in both glucose conditions (Supplemental Figure S1).

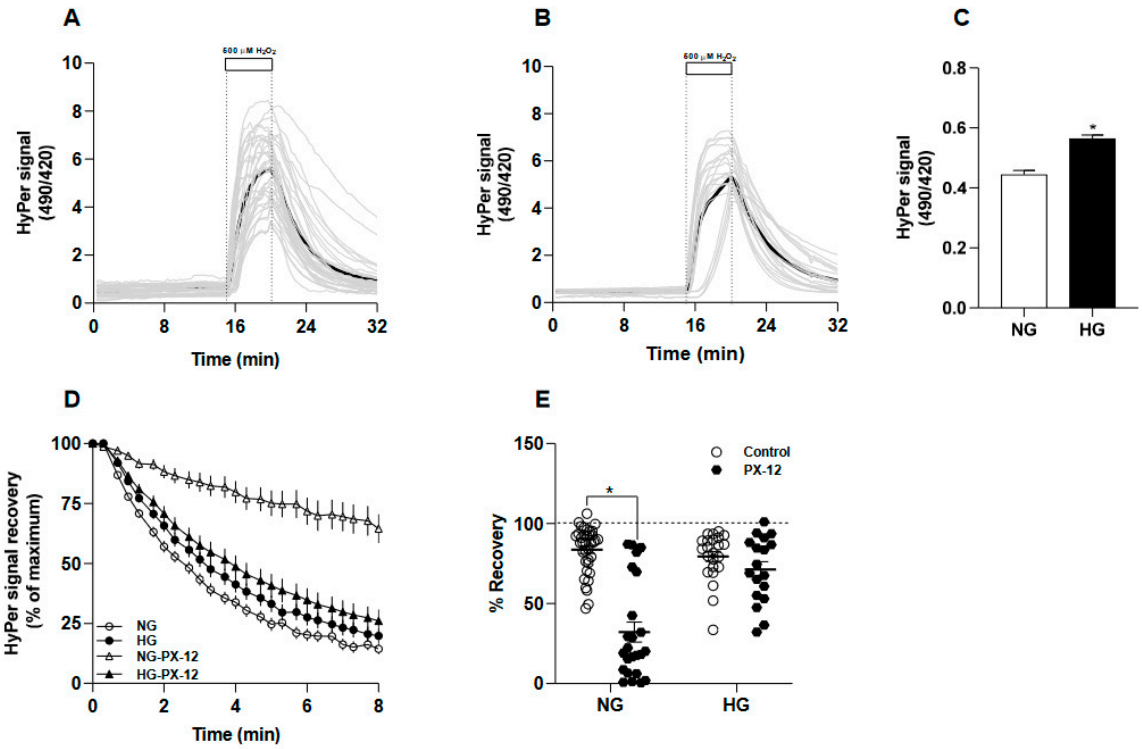


**Figure 1.** Redox responses of HyPer-expressing human fibroblasts cultured at 5 and 25 mM glucose. In A, the time courses of 37 single-cell recordings of HyPer obtained from cells maintained at 5 mM glucose (NG) are shown with grey lines and the average of this group is depicted by a black line. A white box and do ed line indicate the moment and period of exposure to 500 M H2O2. In B, similar to A, but here 23 single-cell recordings belong to fibroblasts maintained at 25 mM glucose (HG), time-courses are represented by grey lines and the application of 500 M H2O2 pulse is indicated by the white box and do ed line on the plot. In both cases, imaging data was collected from four independent experiments. C, a comparison of baseline values of the biosensor obtained from NG-fibroblasts (white bar) and HG-fibroblasts (black bar). Basal values of HyPer were collected from 5-6 random fields from each coverslip, a procedure that was repeated in four independent experiments. This procedure rendered an overall of 129 and 133 cells for NG and HG, respectively. Data correspond to the average ± SE, and the asterisk represents the significant difference between the groups by t-student's test. In D, HyPer signal recovery was obtained right after H2O2 removal, when biosensor is oxidized and present the maximal signal. Data corresponds to the average ± SE of 37 cells for NG (empty circles), 23 cells for HG (filled circles). The contribution of disulfide bond reduction activity to the biosensor recovery was assessed by including 1 M PX-12 to buffer used to wash the hydrogen peroxide out. For these data, the average ± SE of 24 recordings for NG-PX-12 (empty triangles) and 23 cells for HG-

 doi:10.20944/preprints202312.1141.v1



PX-12 (filled triangles) are presented. E, a comparison of the recovery observed in the four groups from D, data correspond to average ± SE. The asterisk indicates significant differences between the groups by one-way ANOVA, Bonferroni post-hoc.Another aspect we evaluated with this molecular device was the recovery rate that the HyPer experiences after removing the oxidative pulse. This recovery phase corresponds to the disulfide bond reduction activity present at the cytoplasm that seems to be quite similar in fibroblasts maintained in normal glucose, which recovered 83.7 ± 0.4% of the signal compared with fibroblasts at high glucose that recovered 79.4 ± 0.7% (Figure 1D). Our next step was to add PX-12, an inhibitor of the cytosolic thioredoxin-1, to unveil the contribution of the thioredoxin system to the reduction of the biosensor. The recovery of HyPer in NG-fibroblasts was more sensitive to PX-12 than in HG-fibroblasts. In contrast, the former was able to recover only 32 ± 1%, and the fibroblast at high glucose reached 73 ± 1% of recovery (Figure 1E), indicating that the reduction of the oxidized biosensor at the cytoplasm of HG-fibroblasts was insensitive to the thioredoxin inhibition.

### *3.2. Redox effects of Selenium compounds on dermic fibroblasts*

To select a non-cytotoxic concentration of selenium and to be compatible with the entire period that fibroblasts need to secret ECM, which takes between seven to ten days after confluency, we first evaluated cellular viability for three selenium compounds: sodium selenite (SS, $Na_2SeO_3$), Selenocysteine (SeCys) and Selenomethionine (SeMet). The analysis of dose-response curves rendered $LC_{50}$ values for SS of 5.7 ± 0.7 μM in NG-fibroblasts and 5.8 ± 0.6 μM in HG-fibroblasts. In the case of selenium amino acids, the $LC_{50}$ values obtained for SeCys in fibroblasts in NG was 16.2 ± 1 μM and in HG was 9.3 ± 1 μM. For SeMet, an $LC_{50}$ of 7.9 ± 2 μM was obtained for fibroblasts in NG, whereas it was 7.9 ± 2 μM for fibroblasts maintained in HG (Supplemental Figure S2). Accordingly, we decided to utilize 1 μM of each selenium compound based on cell viability results and visual inspection of cellular morphology.

Contrary to what we expected, the sustained exposure with 1 mM of selenium, either as a salt or amino acids, induced higher baseline values of the redox biosensor in both conditions, normal and high glucose, than non-treated fibroblasts (Figure 2A). Next, we observed that HyPer biosensor responded faster to 500 μM hydrogen peroxide in NG-maintained fibroblasts treated with SS and SeCys than in non-treated fibroblasts; SeMet showed no significant effect on the biosensor oxidation rate (Figure 2B). In fibroblasts maintained at 25 mM, only selenium amino acids significantly increased the rate of HyPer response by exogenous $H_2O_2$ (Figure 2C) compared with non-treated fibroblasts. In this group, sodium selenite treatment showed no effect.

Preprints (www.preprints.org) | NOT PEER-REVIEWED | Posted: 15 December 2023 doi:10.20944/preprints202312.1141.v1



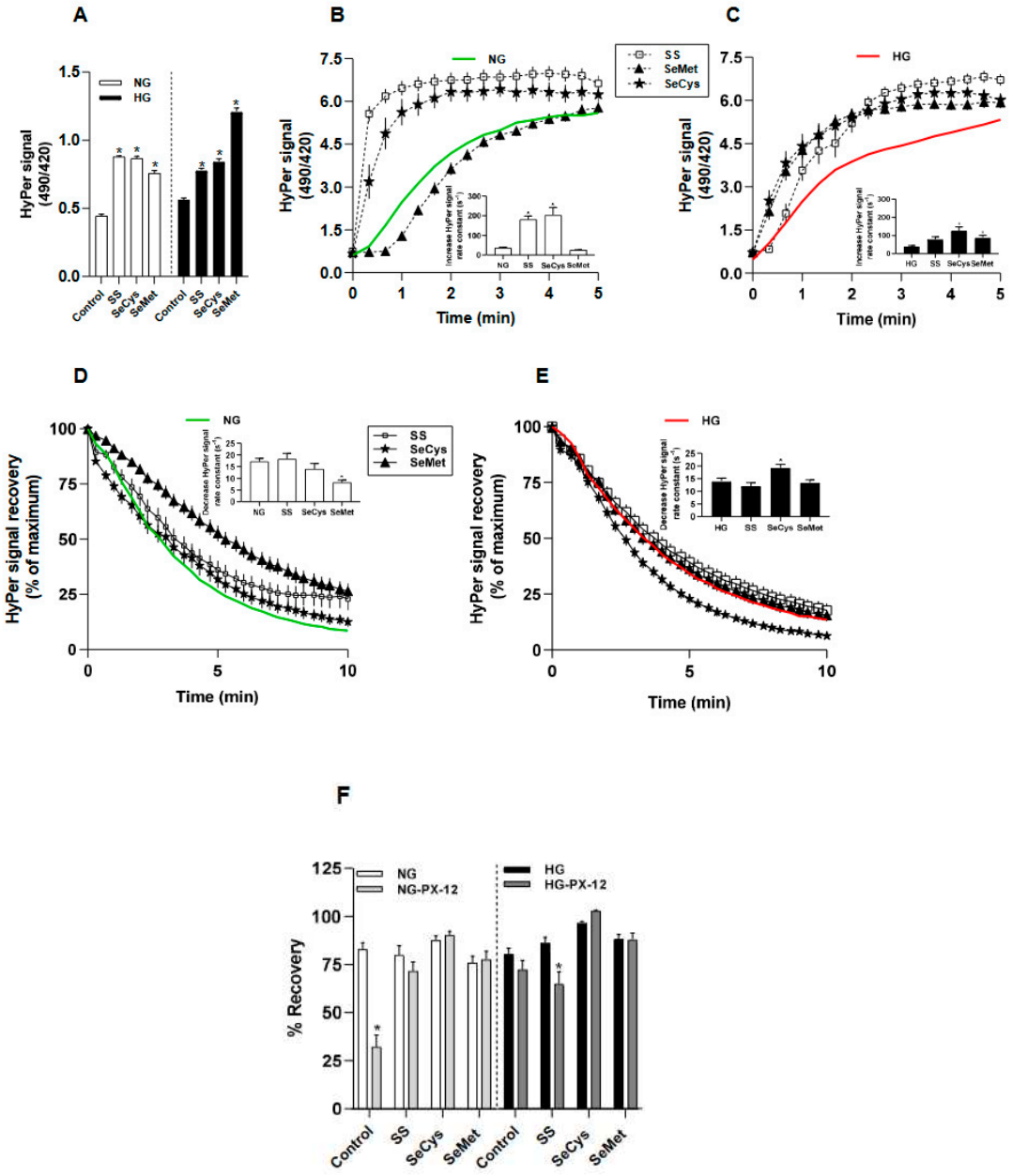


**Figure 2.** Redox alterations induced by the treatment with seleno-compounds in human fibroblast cultured at 5- and 25-mM glucose. A, Comparison of baseline values obtained from HyPerexpressing fibroblasts maintained at 5 (white bars) and 25 mM glucose (filled bars) and treated for ten days with sodium selenite (SS, 1 μM), selenocysteine (SeCys, 1 μM) or selenomethionine (SeMet, 1 μM). For this, baseline values 136 to 170 cells were collected from four independent experiments. Data correspond to the average ± SE, and the asterisks represent the significant difference between the treated groups versus non treated by one-way ANOVA, with post-hoc Bonferroni. B, the time course of HyPer signal increase in NG-fibroblasts upon hydrogen peroxide exposure. Data correspond to the average ± SE of 37 cells for NG (green line), 29 cells for NG-$Na_2SeO_3$ (empty square), 23 cells for NG-SeCys (filled stars) and 37 cells for NG-SeMet (filled triangles) conditions. The inset graph shows the rate constants (b) obtained by data fi ing to the function $HyPer\ ratio = (Maximal - baseline) * e$ . The asterisk indicates significant differences between the treated and non-treated groups by Kruskall-Wallis, Dunn post-hoc. C, Identical to B, but here time-courses of HyPer signal increase were obtained from HG-fibroblasts. Data correspond to the average ± SE of 23 cells for HG (red line), 23 cells for HG-

 doi:10.20944/preprints202312.1141.v1



$Na_2SeO_3$ (1 μM) (empty square), 28 cells for HG-SeCys (1 μM) (filled stars) and 33 cells for HG-SeMet (1 μM) (filled triangles) conditions. The inset graph with black bars compares the rate constants obtained as described in B. The asterisk indicates significant differences between the groups by Kruskall-Wallis, Dunn post-hoc. D, the time-courses of HyPer signal recovery obtained from NG-fibroblasts (green line) and subjected to treatments with $Na_2SeO_3$ (empty square), SeCys (filled stars) and SeMet (filled triangles). Data are expressed as the percentage of the maximal signal obtained from the oxidized biosensor and correspond to average ± SE. The inset graph shows the rate constants (b) obtained by fi ing each single-cell recording to an exponential decay function. E, similar to D, with the difference that here data correspond to HGfibroblasts and the same symbols for the treatments works. The asterisk indicates significant differences between the NG between HG with selenocompounds groups by Kruskall-Wallis, Dunn post-hoc. F. The recovery expressed as percentage is compared in the presence or absence of the thioredoxin-1 inhibitor, PX-12 (1 μM, gray bars). In the left panel, biosensor recovery time-courses obtained from NG-fibroblasts treated or not with seleno compounds. In the right panel, the percent of recovery obtained from HG-fibroblasts. Data correspond to average ± SE and the asterisks indicate significant differences between the groups by one-way ANOVA, Bonferroni post-hoc.

Next, we analyzed the effect of the selenium compounds on the recovery rate of the biosensor. In NG-fibroblasts, the treatments with selenium compounds did not affect the recovery rate of HyPer signal after $H_2O_2$-induced oxidation except SeMet, which diminished the reducing capacity of the cytoplamic environment, decreasing the rate of HyPer recovery from 17.2 ± 1 $s^{-1}$ in non-treated to 8.2 ± 1 $s^{-1}$ in SeMet treated of NG-fibroblasts (Figure 2D). In HG-fibroblasts, we found that only the treatment with SeCys accelerated the rate of the biosensor recovery from 13.9 ± 1 $s^{-1}$ in non-treated to 19.2 ± 1 $s^{-1}$ in SeCys-treated HG-fibroblasts (Figure 2E). Intriguingly, when we tested the sensitivity to PX-12 of the recovery phase in seleno-treated fibroblasts (Supplemental Figure S3), we found in NG-fibroblasts that culturing the cells with all three selenium compounds abolished the inhibitory effect that PX-12 exerts on the reduction of the oxidized biosensor (Figure 2F). A similar response was observed in HG-fibroblasts cultured in the presence of seleno-amino acids; however, sodium selenite sensitized these cells to PX-12, significantly decreasing the recovery degree oxidized biosensor (Figure 2G).

In summary, we could not observe a clear pattern of the redox impact of selenium on human fibroblasts. Nevertheless, the ratio signal of the HyPer biosensor at the baseline, which represents the thiol/disulfide balance at the steady state, was significantly increased by all types of selenium evaluated, independently of the glucose level in the culture conditions. Thus, we explored the possibility that the selenium treatment could modify the transcript levels of some cytoplasmic redox enzymes. The treatment with selenomethionine increased the abundance of glutathione reductase-1, thioredoxin reductase-1 and peroxiredoxin-1 in NG-fibroblasts, although these changes did not reach statistical significance. We only found a significant decrease in the expression of aquaporin-1 in HG-fibroblast treated with SeMet (Supplemental Figure S4).

### *3.3. Effects of high glucose culture and selenium compounds on the abundance, thickness, and crosslinking of fibers secreted by dermal fibroblasts*

To observe the ultrastructure of secreted ECM by fibroblasts, cell bodies were removed, and the remaining material deposited on the surface was prepared for scanning under electronic microscopy and for collagen staining with Picrus Sirius Red. A comparative panel of representative images of extracellular collagen stained with pictures of Sirius red is shown in Figure 3A. After the analysis of the total surface covered by red stain, we observed a slight but significant decrease in the amount of collagen secreted by HG-fibroblasts (from 22 ± 1% in NG-fibroblasts to 15 ± 1% in HG-fibroblasts, t-Student's test). Regarding the effect of selenium compounds, the treatment with SeCys induced a more abundant presence of collagen in NG-fibroblasts (32 ± 4%), an effect that was not observed in HG-fibroblasts (15 ± 1%). On the contrary, SeMet induced a dramatic diminishment in the collagen-covered extracellular surface of fibroblast maintained in either normal or high glucose, 4.5 ± 0.4% and 4.9 ± 0.7%, respectively (Figure 3B).

Preprints (www.preprints.org) | NOT PEER-REVIEWED | Posted: 15 December 2023 doi:10.20944/preprints202312.1141.v1



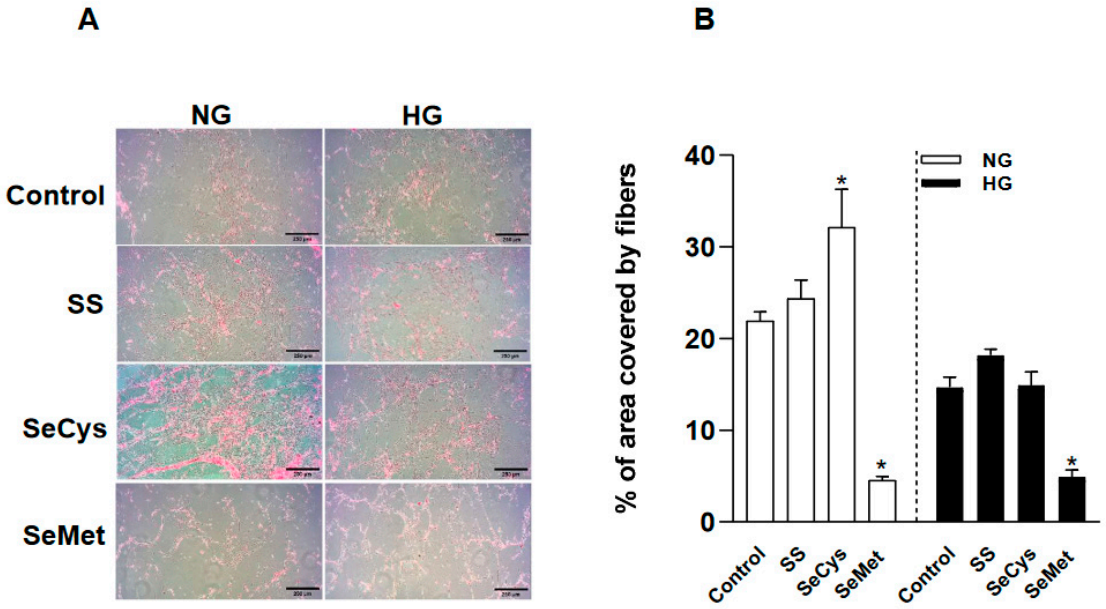


**Figure 3.** Effect of selenium compounds treatments on the abundance of extracellular collagen secreted by CCD1068Sk cells. In A, the panel of images show the staining with Picrus Sirius Red on the surface that CCD1068sK cells left after decellularization. The black bar in the lower right corner of each image represents 250 µm. NG and HG fibroblasts were treated with 1 M sodium selenite (SS); Selenocysteine (SeCys) and selenomethionine (SeMet). B, the area covered by the staining with Picrus Sirius Red was quantified by following a sequential step that included background subtraction/RGB stack/threshold in image J software. Experiments were conducted in triplicate and repeated in three times. Data are expressed as average ± SE. The asterisk indicates significant differences between NG and HG with selenium compounds groups by Kruskall-Wallis, Dunn posthoc. .

Next, we examined the thickness, branching and crosslinking of extracellular fibers by Scanning Electronic Microscopy (Figure 4A). By visual inspection of SEM images, we could perform precise measurements of 20 nm thickness for individual fibers, albeit our analysis was blind to thinner fibers, the population of fibers deposited by HG-fibroblasts were thicker than those produced by NG-fibroblasts (Figure 4B). This morphological feature in high glucose was not affected by sodium selenite and SeCys. However, a significant increase in fiber thickness was observed in fibroblast treated with SeMet, an effect also noted in NG-fibroblasts. To compare the branching level for each fiber, we only considered a maximum of 30 branches per fiber, an upper limit that included more than 90% of the universe of observations; data distribution can be found in the supplemental figure 5. With this approach, we noted that HG-fibroblasts produced fibers with more branches than NG-fibroblasts (Figure 4C). The treatment with SeCys significantly increased the number of branches per fiber in HG-fibroblasts, whereas in NG-fibroblast, SeMet induced a similar effect. SeMet consistently increased the percentage of fibers with more than 30 branches, from 5.4% in non-treated NG-fibroblasts to 10% in treated with SeMet. SeCys, on the other hand, increased this type of fiber population from 7.7% to 9.4% in HG-fibroblasts. Alternatively, the number of nodes with three cross-links was determined for each condition. SeMet increased the number of these nodes in the fibers secreted by NG-fibroblasts and SeCys produced a similar effect in HG-fibroblasts (Figure 4D).

Preprints (www.preprints.org) | NOT PEER-REVIEWED | Posted: 15 December 2023 doi:10.20944/preprints202312.1141.v1



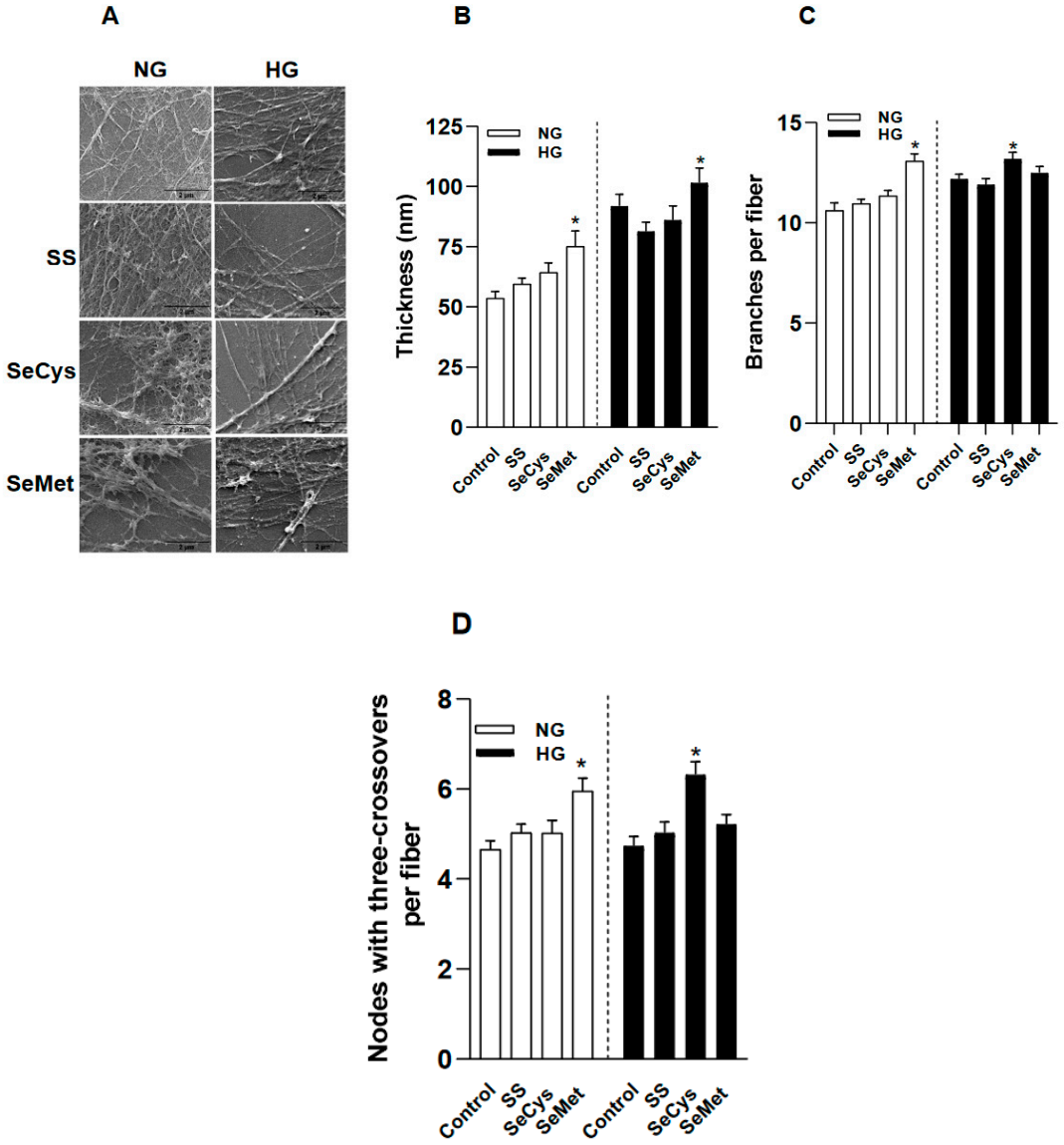


**Figure 4.** Effect of high glucose and selenium compounds on thickness, numbers of branches and crosslinking of fibers secreted by dermal fibroblasts. CCD1068sK cells were maintained under the collagen synthesis protocol for 10 days in normal glucose (NG, 5 mM) and high glucose (HG, 25 mM) conditions with ascorbic acid (155 μM) and selenium compounds 1 μM: sodium selenite (SS); Selenocysteine (SeCys) and selenomethionine (SeMet). Subsequently, the samples were decellularized and fixed. A, a set of representative images taken by scanning electron microscope at 50,000x. The black bar in the lower right corner of each image represents 2 μm. In B, the graph compares the thickness of at least 50 fibers per condition, white bars to the left panel for NG and black bars to the right for HG. C, the graph compares the number of branches obtained after skeletonizing the images, only branches associated to an intersection were considered, at least 9,000 intersections were used to this analysis. D, the number of crosslinking nodes were obtained from skeletonized images. Data represents the average ± SE of from two to three independent trials. The asterisk indicates significant differences between selenocompounds in NG or HG conditions by KruskallWallis, Dunn post-hoc.

*3.4. Selenium compounds treatment improved endothelial cell migration on extracellular matrix synthesized by HG-fibroblasts and purified collagen fibers subjected to glycation*

Preprints (www.preprints.org) | NOT PEER-REVIEWED | Posted: 15 December 2023 doi:10.20944/preprints202312.1141.v1



To test if the morphological changes observed in the extracellular matrix generated by HG-fibroblasts had some relevance for tissue regeneration, we performed wound healing assays with TIME endothelial cells (ECs), which are derived from the microvascular bed of the dermis (Figure 5A).

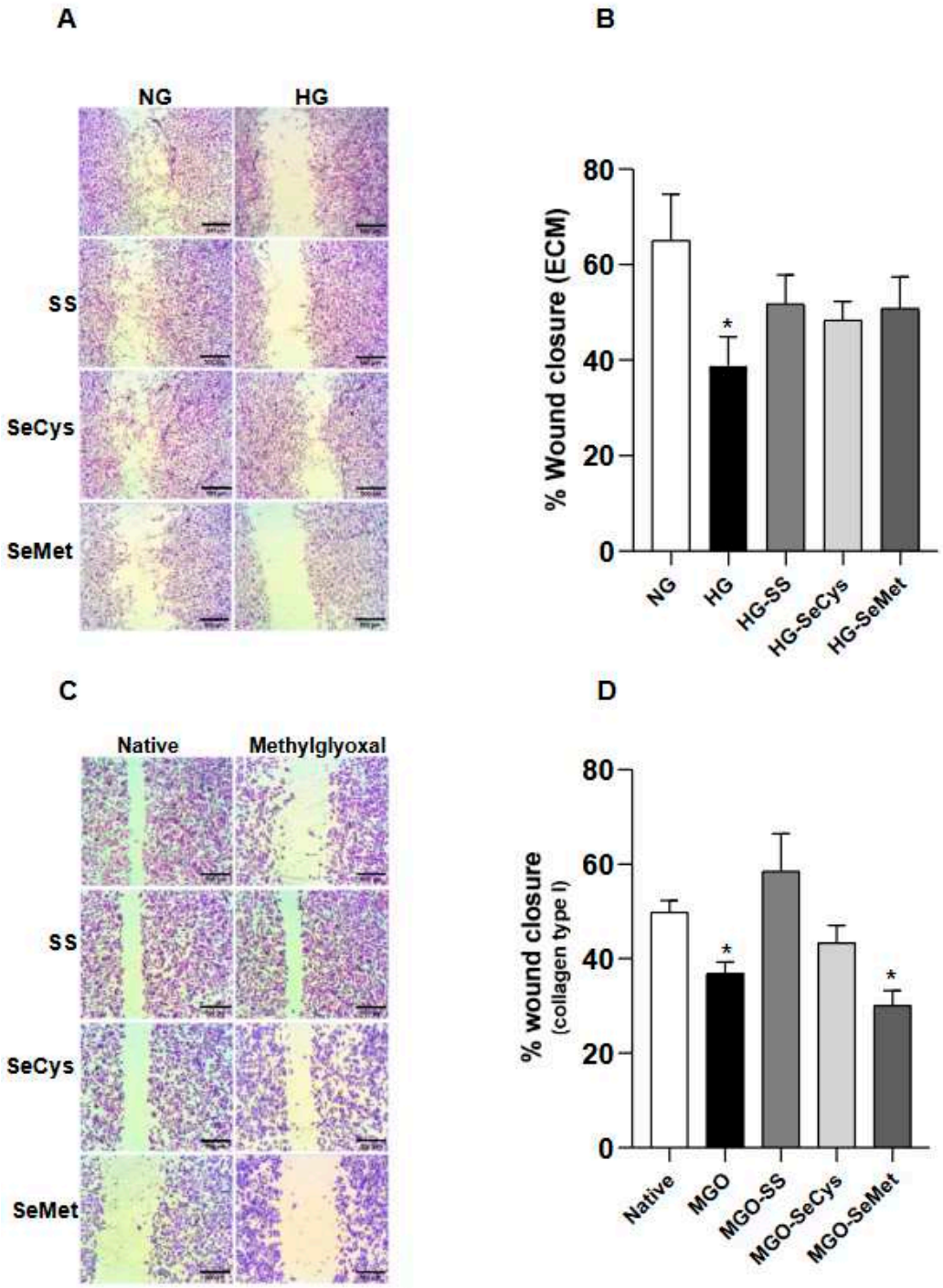


**Figure 5.** Selenium compounds treatments partially improve the surface for cellular migration: wound assay with microvascular endothelial cells. A, a panel of bright field images was taken at 4x magnification of wound assays performed in TIME cell after 8 hours growing on decellularized matrix (ECM) produced by CCD1068sK fibroblasts maintained under normal (NG, 5 mM) and high glucose (HG, 25 mM) conditions with the selenocompounds. The black bars in the lower right corner of each image represent 500 μm. In B, the quantification of the gap area filled by TIME cells (p6-10). The wound closure percentage is the average ± SE of 18 observations from three independent experiments.

 doi:10.20944/preprints202312.1141.v1



The asterisk indicates significant differences in the treatments compared to the NG group by Kruskall-wallis, post-hoc Dunn. C. Similar to A, TIME cells were seeded on purified collagen type I treated or not with Methylglyoxal (MGO) and selenium compounds. D, the quantification of the gap area filled by TIME cells (p6-10). Data represents the average ± SE from 18 observations from three independent experiments. The asterisk indicates significant differences in the treatments compared to the Native group by Kruskall-wallis, post-hoc Dunn. .

Our first finding indicates that ECs were less effective in closing the gap on ECM secreted by HG-fibroblasts compared to the ECM secreted by NG-fibroblasts (65 ± 10% for NG; 39 ± 6% for HG). The extent of wound closure improved in ECM of HG-fibroblasts when they were exposed to the selenium compound treatments (Figure 5B). To know the contribution of collagen glycation as a factor in the reduced wound closure percentage observed in ECM secreted by HG-fibroblasts, we worked with purified human Type I collagen, which was left to polymerize overnight in the presence of the glycant agent, methylglyoxal, with or without the selected selenium compounds (Figure 5C). With this in vitro approach, we found that ECs migrated less on collagen surfaces exposed to methylglyoxal and that the treatments with sodium selenite and SeCys dissipated this effect. In contrast, the presence of SeMet was ineffective in improving the EC migration on glycated surfaces (Figure 5D). These pieces of evidence suggest that collagen glycation is important for endothelial migration and that selenite and SeCys somehow interfere with the chemical modification of collagen, such as glycation improving cellular recruitment.

## 4. Discussion

The production of collagen by fibroblasts is central to the generation of ECM. This entire process, from the intracellular collagen biosynthesis to the extracellular maturation of collagen fibrils, is subjected to environmental redox factors. In this work, we examined the differential impact of long-term exposure with three forms of selenium compounds: inorganic, as sodium selenite and organic, in the form of amino acids, Se-cysteine and Se-methionine, on living fibroblasts monitoring the thiol/disulfide bond balance of cytosolic proteins and the way that the intracellular machinery responds to an oxidant challenge and restore oxidized proteins by observing the kinetic of the fluorescent redox biosensor, HyPer. With this approach, we found subtle, although significant, differences in the biosensor signal at steady state and the sensitivity to the thioredoxin inhibitor, PX-12, in HG-fibroblasts compared to NG-fibroblasts. Furthermore, secreted ECM was visualized by SEM, which helped determine that fibers secreted by HG-fibroblast were thicker and more cross-linked than those secreted by NG-fibroblasts. Finally, by doing a migration assay with endothelial cells on these surfaces, generated by NG- and HG-fibroblasts, we found that ECs migrated slower on the ECM secreted by HG-fibroblasts than on the matrix secreted by NG-fibroblasts. Our results indicated that despite the morphological changes of ECM and the intracellular redox perturbations induced by culturing fibroblasts at high glucose, the treatment with selenium, in all the forms evaluated here, improved the endothelial migration not by counteracting the redox balance nor by modifying the ECM framework but by interfering with glycation on collagen fibers.

### *4.1. Long-term exposure of Selenium compounds and its Antioxidant Effects*

Despite selenium has a concrete biological role by being incorporated into several redox enzymes in the form of seleno-aminoacids (Se-Cys and Se-Met), several groups have reported a biphasic dose-response curve that shows that high doses of selenium become toxic in cellular [43–45] and animal [46–48] models. The most extended exposure period at the cellular level does not exceed four days [49–51]. In this study, we used the two mentioned amino acids and the inorganic form, sodium selenite, at 1 μM for 10 days, maintaining cellular viability. Curiously, mammalian cells seem more tolerant to selenium supplementation if they are subjected to stress. For instance, trophoblasts (HTR8/SVneo), presented loss of their cellular integrity at 5.5 mM of sodium selenite or 6.2 mM selenomethionine within 24 hours; however, the same concentrations had a protective effect in cells treated with 15 μM menadione, to induce oxidative stress [52]. This phenomenon perhaps reflects the

 doi:10.20944/preprints202312.1141.v1



convergence of two mechanisms triggered in stressed cells, one that involves the canonical activation of transcriptional factors like Nrf-2 [53], HO [54], Hif-1 [55], among others, which regulate the abundance of transcripts for antioxidant enzymes and another set of specific mechanisms associated to the usage of selenium amino acid during protein translation, which are concentrated on the regulation of transfer RNASec [22,56,57], essential for the biosynthesis of selenoproteins [58,59].

High glucose in the culture condition promotes an oxidative intracellular environment by diverse mechanisms that include inhibition of antioxidant defenses [60], and increased ROS production by mitochondria [61] or NOX [62]. Here, we observed an increase in the basal ratio signal of HyPer in HG-fibroblasts compared to NG-fibroblasts. Unexpectedly, the long-term treatment with the selenium compounds pushes the redox balance toward an even more oxidized biosensor than high glucose did. In this context, sodium selenite (20 μM, 48 hrs) reduced cellular apoptosis, decreased production of reactive oxygen species, assessed with 2,7-dichlorofluorescein diacetate (DCFH-DA), and increased activity of the glutathione peroxidase enzyme on rat cardiomyocytes maintained under high glucose conditions (25 mM) [63]. A similar effect was reported in retina cells from pigs maintained between 5 to 80 mM of glucose; the treatment with sodium selenite (250 nM, 24 hrs) reduced caspase-mediated apoptosis and decreased ROS production [64].

On the contrary, human dermic fibroblasts showed no morphological differences between the two glucose levels used here; they proliferated at a similar rate. At this point, it is relevant to establish that high glucose did not affect cellular viability. We observed that HG-fibroblasts were more sensitive to the treatment with selenium than NG-fibroblasts. For example, the $LC_{SE\text{-}Cys}$ was 16.2 ± 1 mM for NG-fibroblasts. In contrast, it was 9.3 ± 1 mM for HG-fibroblasts, indicating that the high glucose condition used here was not working as a cellular stressor for dermic fibroblasts. Thus, it did not promote cellular selenium usage.

### *4.2. Understanding the Impact of Glycation on Secreted Fibers: Exploring Selenium's Role*

Our findings indicate that fibroblasts secrete fibers with different structural properties under high glucose conditions or in the treatment with selenium compounds. All the mentioned conditions provoked an increase in the oxidative tone at the cytoplasm of fibroblasts, and accordingly, all these conditions promoted the secretion of thicker fibers. Particularly, the thickening of collagen is a biological process that depends on the activity of LOX, an amino oxidase-type enzyme, that promotes the crosslinking of tropocollagen fibers to form the collagen fibril by deamination of lysine residues necessary for the formation of covalent bonds between fibers [7]. Although we did not find changes in the abundance of LOX mRNAs (data not shown), we do not discard an increase in the LOX activity by the high glucose. There is evidence that high glucose conditions increase the activity of NADPH oxidase with the concomitant production of $H_2O_2$ [65], events that be linked to stimulation of LOX activity in human endothelial cells [11] that exhibits altered ECM characterized by higher crosslinking of collagen and elastin [10]. In this work, we observed that the treatments with selenium compounds, which promoted a more oxidative tone in fibroblasts than high glucose condition did, improved the ECM for endothelial migration. This effect was also observed in purified collagen fibers subjected to glycation, which indicated that sodium selenite and SeCys could interact with collagen at the molecular level. This type of interaction has been reported with selenium nanoparticles, which decreased the formation of advanced glycation end products by ribose on lactoglobulin protein [66]; this protection is probably due to selenium shields amino groups preventing the formation of the Schiff base [67].

Glycation on collagen fibrils has been associated with impaired cellular migration [68–71]. In most in vitro approaches, massive amounts of glucose or other glycan agents are used on purified collagen fibers. In this work, we studied the ECM generated by dermic fibroblast cultured in 25 mM glucose. This concentration represents the hyperglycemia observed in diabetic patients [72] and is well-tolerated by cultured cells. Under this condition, the ECM covered less area than the secreted by NG-fibroblasts, likely because thicker and more cross-linked fibers produced by HG-fibroblasts tend to be in groups composed of piled-up fibers. Whether this HG-promoted ECM arrangement has a different stiffness compared to the ECM generated by NG-fibroblast is unknown. However, atomic

force microscopy measurements on plantar tissue obtained from diabetic patients indicate an increased stiffness compared with healthy patients [73]. High extracellular glucose leads to the establishment of an ECM with morphological and mechanical properties that impair cell migration. Selenium compounds improved ECM generated by HG-fibroblasts for endothelial cell migration; this positive effect was also observed in methylglyoxal-treated purified collagen fibers, at least with sodium selenite and selenocysteine. Unfortunately, the mechanisms behind this effect are puzzling since selenomethionine, which shares the same valence on the Se atom as selenocysteine, does not affect migration.

From the perspective of migrating endothelial cells, a glycated collagen surface produces changes in the profile expression of integrins, increasing $\alpha$Vβ3 and decreasing $\alpha$2 β1, promoting cellular adhesion [75]. These changes may be linked to impaired angiogenesis [74] that contributes to perpetuating dermic lesions in decompensated diabetic patients. Given the potential benefits of selenium compounds as promoters of migration under glycation and their ability to impede the formation of AGEs [66,67], they emerge as an alternative for treating chronic wounds, such as diabetic foot ulcers. A transdermal patch with selenium and chitosan nanoparticles significantly reduced inflammation in 7 days in an animal model for wound healing study; this procedure also improved neovascularization and collagen formation at day 21 [25]; similar results were observed by applying a hydrogel, consisting of selenium nanoparticles embedded in cellulose-gelatin, that increased collagen deposition, angiogenesis, and fibroblast activation in rats [29]. Combination with other compounds has also shown that selenium in a hydrogel structure and zinc can improve full-thickness histopathological indices of wound healing in pediatric lesions [76].

## 5. Conclusions

The effects of high glucose on cellular redox status are not mitigated by selenium compound treatment, nor are the structural changes in fibers secreted by fibroblasts. Nevertheless, selenium compounds transform the extracellular matrices secreted by fibroblasts cultured in high glucose in a more transitable surface for microvascular endothelial cells.

**Supplementary Materials:** The following supporting information can be downloaded at the website of this paper posted on Preprints.org.

**Author Contributions:** Conceptualization, C.K. and O.P.; methodology, C.K., A.R. and M.H.; formal analysis, C.K. and O.P.; resources, O.P., R.P. and C.A.; writing—original draft preparation, C.K., O.P. and S.S.; writing—review and editing, C.K., O.P. and S.S.; supervision, O.P. and R.P.; All authors have read and agreed to the published version of the manuscript.

**Funding:** This research was funded by ANID-FONDEF-IT18I0021 (O.P.), FONDECYT-1212026 (C.A.), PhD fellowship-ANID 2118077 (C.K.).

**Institutional Review Board Statement:** Not applicable

**Informed Consent Statement:** Not applicable.

**Acknowledgments:** We thank the ABCVital project, an institutional initiative that contributes to our lab creation.

**Conflicts of Interest:** The authors declare no conflict of interest.

## References

1. Danaei G, Finucane M, Lu Y, Singh G, Cowan M, Paciorek C, et al. National, regional, and global trends in fasting plasma glucose and diabetes prevalence since 1980: systematic analysis of health examination surveys and epidemiological studies with 370 country-years and 2·7 million participants. Lancet 2011,378,31–40. DOI: 10.1016/S0140-6736(11)60679-X
2. Rahbar S, Blumenfeld O, Ranney HM. Studies of an unusual hemoglobin in patients with diabetes mellitus. Biochem Biophys Res Commun 1969,36,838–43. DOI: 10.1016/0006-291x(69)90685-8
3. Škrha J, Šoupal J, Škrha J, Prázný M. Glucose variability, HbA1c and microvascular complications. Rev Endocr Metab Disord 2016,17,103–10. DOI: 10.1007/s11154-016-9347-2
4. Muir R, Forbes S, Birch DJS, Vyshemirsky V, Rolinski OJ. Collagen Glycation Detected by Its Intrinsic Fluorescence. J Phys Chem B 2021,125,11058–66. DOI: 10.1021/acs.jpcb.1c05001

5. Saremi A, Howell S, Schwenke DC, Bahn G, Beisswenger PJ, Reaven PD. Advanced Glycation End Products, Oxidation Products, and the Extent of Atherosclerosis During the VA Diabetes Trial and Follow-up Study. Diabetes Care 2017,40,591–8. DOI: 10.2337/dc16-1875
6. Genuth S, Sun W, Cleary P, Gao X, Sell D, Lachin J, et al. Skin advanced glycation end products glucosepane and methylglyoxal hydroimidazolone are independently associated with longterm microvascular complication progression of type 1 diabetes. Diabetes 2015,64,266–78. DOI: 10.2337/db14-0215
7. Gelse K, Pöschl E, Aigner T. Collagens--structure, Function, and Biosynthesis. Adv Drug Deliv Rev 2003,55,1531–46.
8. Salo AM, Myllyharju J. Prolyl and lysyl hydroxylases in collagen synthesis. Exp Dermatol 2021,30,38–49. DOI: 10.1016/j.addr.2003.08.002
9. Liu R, Desai L. Reciprocal regulation of TGF-β and reactive oxygen species: A perverse cycle for fibrosis. Redox Biol 2015,6,565–577. DOI: 10.1016/j.redox.2015.09.009
10. Du X, Matsumura T, Edelstein D, Rossetti L, Zsengellér Z, Szabó C, et al. Inhibition of GAPDH activity by poly(ADP-ribose) polymerase activates three major pathways of hyperglycemic damage in endothelial cells. J Clin Invest 2003,112,1049–57. DOI: 10.1172/JCI18127
11. Guadall A, Orriols M, Alcudia J, Cachofeiro V, Martinez-Gonzalez J, Rodriguez C. Hypoxia-induced ROS Signaling Is Required for LOX Up-Regulation in Endothelial Cells. Front Biosci (Elite Ed) 2011, 3, 955–67. DOI: 10.2741/e301
12. Papachroni KK, Piperi C, Levidou G, Korkolopoulou P, Pawelczyk L, Diamanti-Kandarakis E, et al. Lysyl oxidase interacts with AGE signalling to modulate collagen synthesis in polycystic ovarian tissue. J Cell Mol Med 2010, 14, 2460–9. DOI: 10.1111/j.1582-4934.2009.00841.x
13. Lee K, Chiang M, Chen P, Ho M, Lee H, Lee H, et al. The effect of low-level laser irradiation on hyperglycemia-induced inflammation in human gingival fibroblasts. Lasers Med Sci 2018, 1–8. DOI: 10.1007/s10103-018-2675-6
14. Kamml J, Acevedo C, Kammer DS. Advanced-Glycation Endproducts: How cross-linking properties affect the collagen fibril behavior. J Mech Behav Biomed Mater 2023, 148, 106198. DOI: arXiv:2308.05514v1.
15. Dobler D, Ahmed N, Song L, Eboigbodin K, Thornalley P. Increased Dicarbonyl Metabolism in Endothelial Cells in Hyperglycemia Induces Anoikis and Impairs Angiogenesis by RGD and GFOGER Motif Modification. Diabetes 2006, 55, 1961–9. DOI: 10.2337/db05-1634
16. Fairweather-Tait SJ, Bao Y, Broadley MR, Collings R, Ford D, Hesketh JE, et al. Selenium in Human Health and Disease. Antioxid Redox Signal 2011, 14, 1337–83. DOI: 10.1089/ars.2010.3275
17. Brigelius-Flohé R, Maiorino M. Glutathione peroxidases. Biochim Biophys Acta 2013, 1830, 3289–303. DOI: 10.1016/j.bbagen.2012.11.020
18. Kenet G, Freedman J, Shenkman B, Regina E, Brok-Simoni F, Holzman F, et al. Plasma glutathione peroxidase deficiency and platelet insensitivity to nitric oxide in children with familial stroke. Arterioscler Thromb Vasc Biol, 1999, 19, 2017–23. DOI: 10.1161/01.atv.19.8.2017
19. Shi Y, Vanhoutte PM. Macro- and microvascular endothelial dysfunction in diabetes. J Diabetes 2017, 9, 434–49. DOI: 10.1111/1753-0407.12521
20. Peng X, Mandal P, Kaminskyy V, Lindqvist A, Conrad M, Arnér E. Sec-containing TrxR1 is essential for self-sufficiency of cells by control of glucose-derived $H_2O_2$. Cell Death Dis 2014, 5, e1235. DOI:10.1038/cddis.2014.209
21. Wen W, Weiss SL, Sunde RA. UGA Codon Position Affects the Efficiency of Selenocysteine Incorporation into Glutathione Peroxidase-1. Journal of Biological Chemistry 1998, 273, 28533–41. DOI: 10.1074/jbc.273.43.28533
22. Fradejas-Villar N, Bohleber S, Zhao W, Reuter U, Kotter A, Helm M, et al. The Effect of tRNA[Ser]Sec Isopentenylation on Selenoprotein Expression. Int J Mol Sci 2021, 22, 11454. DOI: 10.3390/ijms222111454
23. Sengupta A, Lichti U, Carlson B, Ryscavage A, Gladyshev V, SH Y, et al. Selenoproteins are essential for proper keratinocyte function and skin development. PLoS One, 2010, 5, e12249. DOI: 10.1371/journal.pone.0012249
24. Heo JS. Selenium-Stimulated Exosomes Enhance Wound Healing by Modulating Inflammation and Angiogenesis. Int J Mol Sci 2022, 23, 11543. DOI: 10.3390/ijms231911543
25. Altememy D, Javdani M, Khosravian P, Khosravi A, Moghtadaei Khorasgani E. Preparation of Transdermal Patch Containing Selenium Nanoparticles Loaded with Doxycycline and Evaluation of Skin Wound Healing in a Rat Model. Pharmaceuticals 2022, 15, 1381. DOI: 10.3390/ph15111381
26. Song SH, Kim JE, Koh EK, Sung JE, Lee HA, Yun W Bin, et al. Selenium-loaded cellulose film derived from Styela clava tunic accelerates the healing process of cutaneous wounds in streptozotocin-induced diabetic Sprague–Dawley rats. Journal of Dermatological Treatment 2018, 29, 606–16. DOI: 10.1080/09546634.2018.1425357
27. El-Sayed H, Morad MY, Sonbol H, Hammam OA, Abd El-Hameed RM, Ellethy RA, et al. Myco-Synthesized Selenium Nanoparticles as Wound Healing and Antibacterial Agent: An In Vitro and In Vivo Investigation. Microorganisms 2023, 11, 2341. DOI: 10.3390/microorganisms11092341

28. Luo L, Wang Y, Zhang S, Guo L, Jia G, Lin W, et al. Preparation and characterization of selenium-rich polysaccharide from Phellinus igniarius and its effects on wound healing. Carbohydr Polym 2021, 264, 117982. DOI: 10.1016/j.carbpol.2021.117982
29. Mao L, Wang L, Zhang M, Ullah MW, Liu L, Zhao W, et al. In Situ Synthesized Selenium Nanoparticles-Decorated Bacterial Cellulose/Gelatin Hydrogel with Enhanced Antibacterial, Antioxidant, and Anti-Inflammatory Capabilities for Facilitating Skin Wound Healing. Adv Healthc Mater 2021, 10. DOI: 10.1002/adhm.202100402
30. Muchová J, Hearnden V, Michlovská L, Vištejnová L, Zavaďáková A, Šmerková K, et al. Mutual influence of selenium nanoparticles and FGF2-STAB® on biocompatible properties of collagen/chitosan 3D scaffolds: in vitro and ex ovo evaluation. J Nanobiotechnology 2021, 19, 103. DOI: 10.1186/s12951-021-00849-w
31. Webster T, Hassan C. The effect of red-allotrope selenium nanoparticles on head and neck squamous cell viability and growth. Int J Nanomedicine 2016, 11, 3641–54. DOI: 10.2147/IJN.S105173
32. Hoefig CS, Renko K, Köhrle J, Birringer M, Schomburg L. Comparison of different selenocompounds with respect to nutritional value vs. toxicity using liver cells in culture. J Nutr Biochem, 2011, 22, 945–55. DOI: 10.1016/j.jnutbio.2010.08.006
33. Webster TJ, Ramos. Cytotoxicity of selenium nanoparticles in rat dermal fibroblasts. Int J Nanomedicine, 2012, 3907. DOI: 10.2147/IJN.S33767
34. Cukierman E. Preparation of Extracellular Matrices Produced by Cultured Fibroblasts. Curr Protoc Cell Biol, 2002. DOI: 10.1002/cpcb.2
35. Wigg AJ, Phillips JW, Wheatland L, Berry MN. Assessment of cell concentration and viability of isolated hepatocytes using flow cytometry. Anal Biochem 2003, 317, 19–25. DOI: 10.1016/s0003-2697(03)00057-5
36. Belousov V, Fradkov A, Lukyanov K, Staroverov D, Shakhbazov K, Terskikh A, et al. Genetically encoded fluorescent indicator for intracellular hydrogen peroxide. Nat Methods 2006, 3, 281–286. DOI: 10.1038/nmeth866
37. Pouvreau S. Genetically encoded reactive oxygen species (ROS) and redox indicators. Biotechnol J 2014, 9, 282.
38. Meyer AJ, Dick TP. Fluorescent protein-based redox probes. Antioxid RedoxSignal 2010, 13, 621–50.
39. Hernández H, Parra A, Tobar N, Molina J, Kallens V, Hidalgo M, et al. Insights into the HyPer biosensor as molecular tool for monitoring cellular antioxidant capacity. Redox Biol 2018, 16, 188–208. DOI: 10.1002/biot.201300199
40. Pfaffl M. A new mathematical model for relative quantification in real-time RT-PCR. Nucleic Acids Res 2001, 9. DOI: 10.1093/nar/29.9.e45
41. Schindelin J, Arganda-Carreras I, Frise E, Kaynig V, Longair M, Pietzsch T, et al. Fiji: an open-source platform for biological-image analysis. Nat Methods 2012, 9, 676–82. DOI: 10.1038/nmeth.2019
42. Fischer ER, Hansen BT, Nair V, Hoyt FH, Dorward DW. Scanning Electron Microscopy. Curr Protoc Microbiol 2012, 25. DOI: 10.1002/9780471729259.mc02b02s25
43. Wu C, Cui C, Zheng X, Wang J, Ma Z, Zhu P, et al. The Selenium Yeast vs. Selenium Methionine on Cell Viability, Selenoprotein Profile and Redox Status via JNK/P38 Pathway in Porcine Mammary Epithelial Cells. Front Vet Sci 2022, 9. DOI: 10.3389/fvets.2022.850935
44. Na JY, Seok J, Park S, Kim JS, Kim GJ. Effects of selenium on the survival and invasion of trophoblasts. Clin Exp Reprod Med 2018, 45, 10–6. DOI: 10.5653/cerm.2018.45.1.10
45. Gonçalves AC, Barbosa-Ribeiro A, Alves V, Silva T, Sarmento-Ribeiro AB. Selenium compounds induced ROS-dependent apoptosis in myelodysplasia cells. Biol Trace Elem Res 2013, 154, 440–7. DOI: 10.1007/s12011-013-9749-x
46. Raisbeck MF. Selenosis in Ruminants. Veterinary Clinics of North America. Food Animal Practice 2020, 36, 775–89. DOI: 10.1016/j.cvfa.2020.08.013
47. Mihajlović M. [Selenium toxicity in domestic animals]. Glas Srp Akad Nauka Med 1992, 131–44. DOI: 10.1002/9781119693567.ch4
48. O'Toole D, Raisbeck MF. Experimentally Induced Selenosis of Adult Mallard Ducks: Clinical Signs, Lesions, and Toxicology. Vet Pathol 1997, 34, 330–40. DOI: 10.1177/030098589703400409
49. Baker R, Baker S, Rao R. Selenium Deficiency in Tissue Culture: Implications for Oxidative Metabolism. J Pediatr Gastroenterol Nutr 1998, 27, 287–92. DOI: 10.1097/00005176-199810000-00003
50. Baliga M, Wang H, Zhuo P, Diamond A, Schwartz A. Selenium and GPx-1 overexpression protect mammalian cells against UV-induced DNA damage. Bio Trace Elem Res 2007, 115, 227–41. DOI: 10.1007/BF02685998
51. Jobeili L, Rousselle P, Béal D, Blouin E, Roussel A, Damour O, et al. Selenium preserves keratinocyte stemness and delays senescence by maintaining epidermal adhesion. Aging (Albany NY) 2017, 9, 2302–15. DOI: 10.18632/aging.101322
52. Habibi N, Jankovic-Karasoulos T, Leemaqz SYL, Francois M, Zhou SJ, Leifert WR, et al. Effect of Iodine and Selenium on Proliferation, Viability, and Oxidative Stress in HTR-8/SVneo Placental Cells. Biol Trace Elem Res 2021, 199, 1332–44. DOI: 10.1007/s12011-020-02277-7

53. De Spirt S, Eckers A, Wehrend C, Micoogullari M, Sies H, Stahl W, et al. Interplay between the chalcone cardamonin and selenium in the biosynthesis of Nrf2-regulated antioxidant enzymes in intestinal Caco-2 cells. Free Radic Biol Med 2016, 91, 164–71. DOI: 10.1016/j.freeradbiomed.2015.12.011
54. Abo El-Magd NF, Barbosa PO, Nick J, Covalero V, Grignetti G, Bermano G. Selenium, as selenite, prevents adipogenesis by modulating selenoproteins gene expression and oxidative stress–related genes. Nutrition 2022, 93, 111424. DOI: 10.1016/j.nut.2021.111424
55. Acharya S, Nithyananthan S, Thirunavukkarasu C. Selenium Nanoparticles Show Anticancer Activity Through Regulation of HIF-1$\alpha$ and HIF-2$\alpha$ Under Hypoxic Condition in Liver Cancer Cells. DNA Cell Biol 2023, 42, 433–44. DOI: 10.1089/dna.2023.0099
56. Diamond AM, Choi IS, Crain PF, Hashizume T, Pomerantz SC, Cruz R, et al. Dietary selenium affects methylation of the wobble nucleoside in the anticodon of selenocysteine tRNA([Ser]Sec). J Biol Chem 1993, 268, 14215–23. DOI: 10.1016/S0021-9258(19)85229-8
57. Hatfield D, Lee BJ, Hampton L, Diamond AM. Selenium induces changes in the selenocysteine tRNA [Ser]Sec population in mammalian cells. Nucleic Acids Res 199, 19, 939–43. DOI:10.1093/nar/19.4.939
58. Bo¨ck A, Forchhammer K, Heider J, Baron C. Selenoprotein synthesis: an expansion of the genetic code. Trends Biochem Sci 1991, 16, 463–7. DOI: 10.1016/0968-0004(91)90180-4
59. Böck A, Forchhammer K, Heider J, Leinfelder W, Sawers G, Veprek B, et al. Selenocysteine: the 21st amino acid. Mol Microbiol 1991, 5, 515–20. DOI: 10.1111/j.1365-2958.1991.tb00722.x
60. Schulze P, Yoshioka J, Takahashi T, He Z, King G, Lee R. Hyperglycemia promotes oxidative stress through inhibition of thioredoxin function by thioredoxin-interacting protein. J Biol Chem 2004, 279, 30369–74. DOI: 10.1074/jbc.M400549200
61. Krauss S, Zhang C, Scorrano L, Dalgaard L, St-Pierre J, Grey S, et al. Superoxide-mediated activation of uncoupling protein 2 causes pancreatic beta cell dysfunction. J Clin Invest 2003, 112, 1831–42. DOI: 10.1172/JCI19774
62. Brownlee M. Biochemistry and molecular cell biology of diabetic complications. Nature 2001, 414, 813–20. DOI: 10.1038/414813a
63. Liu ZW, Zhu HT, Chen KL, Qiu C, Tang KF, Niu XL. Selenium Attenuates High Glucose-Induced ROS/TLR-4 Involved Apoptosis of Rat Cardiomyocyte. Biol Trace Elem Res 2013, 156, 262–70. DOI: 10.1007/s12011-013-9857-7
64. Bardak H, Uğuz AC, Bardak Y, Rocha-Pimienta J, Delgado-Adámez J, Espino J. Selenium Protects ARPE-19 and ACBRI 181 Cells against High Glucose-Induced Oxidative Stress. Molecules 2023, 28, 5961. DOI: 10.3390/molecules28165961
65. Jover E, Silvente A, Marín F, Martínez-González J, Orriols C, Martinez M, et al. Inhibition of Enzymes Involved in Collagen Cross-Linking Reduces Vascular Smooth Muscle Cell Calcification. FASEB J 2018, 32, 4459–69. DOI: 10.1096/fj.201700653R
66. Du P cheng, Tu Z cai, Wang H, Hu Y ming. Mechanism of Selenium Nanoparticles Inhibiting Advanced Glycation End Products. J Agric Food Chem 2020, 68, 10586–95. DOI: 10.1021/acs.jafc.0c03229
67. Yu S, Zhang W, Liu W, Zhu W, Guo R, Wang Y, et al. The inhibitory effect of selenium nanoparticles on protein glycation in vitro. Nanotechnology 2015, 26, 145703. DOI: 10.1088/0957-4484/26/14/145703
68. Liao H, Zakhaleva J, Chen W. Cells and tissue interactions with glycated collagen and their relevance to delayed diabetic wound healing. Biomaterials, 2009, 30, 1689–96. DOI: 10.1016/j.biomaterials.2008.11.038
69. Morita K, Urabe K, Moroi Y, Koga T, Nagai R, Horiuchi S, et al. Migration of keratinocytes is impaired on glycated collagen I. Wound Repair Regen 2005, 13, 93–101. DOI: 10.1111/j.1067-1927.2005.130112.x
70. Jeannesson P. Impact of carbamylation and glycation of collagen type I on migration of HT1080 human fibrosarcoma cells. Int J Oncol 2012. DOI: 10.3892/ijo.2012.1393
71. Kuzan A, Michel O, Gamian A. Glycation of Matrix Proteins in the Artery Inhibits Migration of Smooth Muscle Cells from the Media to the Intima. Folia Biol (Praha) 2017, 63, 105–14. PMID: 28805560.
72. Mustafa OG, Haq M, Dashora U, Castro E, Dhatariya KK. Management of Hyperosmolar Hyperglycaemic State (HHS) in Adults: An updated guideline from the Joint British Diabetes Societies (JBDS) for Inpatient Care Group. Diabetic Medicine 2023 , 40. DOI: 10.1111/dme.15005
73. Kwak Y, Kim J, Lee KM, Koo S. Increase of stiffness in plantar fat tissue in diabetic patients. J Biomech 2020, 107, 109857. DOI: 10.1016/j.jbiomech.2020.109857
74. Francis-Sedlak M, Moya M, Huang J, Lucas S, Chandrasekharan N, Larson J, et al. Collagen Glycation Alters Neovascularization in Vitro and in Vivo. Microvasc Res 2010, 80, 3–9. DOI: 10.1016/j.mvr.2009.12.005
75. Frank S, Cicalese S, Solomon D, Morss A. Glycated Collagen and Altered Glucose Increase Endothelial Cell Adhesion Strength. J Cell Physiol 2013, 228, 1727–36. DOI: 10.1002/jcp.24313
76. Ruan Q, Yuan L, Gao S, Ji X, Shao W, Ma J, et al. Development of ZnO/selenium/selenium nanoparticles embedded chitosan-based anti-bacterial wound dressing for potential healing ability and nursing care after paediatric fracture surgery. Int Wound J 2023, 20, 1819–31. DOI: 10.1111/iwj.13947